Letter to the Editor

VLT and HST observations of a candidate high redshift elliptical galaxy in the Hubble Deep Field South[*]

M. Stiavelli[1,2,6], **T. Treu**[1,2], **C.M. Carollo**[3][**], **P. Rosati**[4], **R. Viezzer**[4], **S. Casertano**[1,6], **M. Dickinson**[1], **H. Ferguson**[1], **A. Fruchter**[1], **P. Madau**[1], **C. Martin**[1], and **H. Teplitz**[5]

[1] Space Telescope Science Institute, 3700 San Martin Dr., MD 21218, USA (mstiavel@stsci.edu, treu@stsci.edu)
[2] Scuola Normale Superiore, Piazza dei Cavalieri 7, I-56126 Pisa, Italy (mstiavel@astro.sns.it, treu@cibs.sns.it)
[3] Johns Hopkins University, 3701 San Martin Dr., MD 21218, USA (marci@pha.jhu.edu)
[4] European Southern Observatory, Karl-Schwarzschild Strasse 2, D-85748 Garching, Germany (prosati@eso.org)
[5] Goddard Space Flight Center, Greenbelt, MD 20771, USA (hit@binary.gsfc.nasa.gov)
[6] On assignment from the Space Science Department of the European Space Agency

Abstract. The combined use of the ESO Very Large Telescope (VLT) UT1 Science Verification (SV) images and of the Hubble Space Telescope (HST) Hubble Deep Field South observations allows us to strengthen the identification as a candidate elliptical galaxy of the Extremely Red Object HDFS 223251-603910 previously identified by us on the basis of NICMOS and Cerro Tololo Interamerican Observatory imaging. The photometry presented here includes VLT data in U, B, V, R, I, a STIS unfiltered image, NICMOS J, H, and K band data, thus combining the 16.5 hours of VLT SV exposures with 101 hours of HST observing. The object is detected in all images except the VLT U band and is one of the reddest known with B-K$= 9.7 \pm 0.5$. We consider a wide range of models with different ages, metallicities, star formation histories and dust content, and conclude that the observed spectral energy distribution agrees best with that of an old elliptical galaxy at redshift just below 2. Alternative possibilities are discussed in light of their likelihood and of the perspective of spectroscopic confirmation.

Key words: galaxies: elliptical and lenticular, cD – galaxies: evolution – galaxies: formation – infrared: galaxies – cosmology: observations

1. Introduction

The formation process of elliptical galaxies is still unknown. Direct observations of elliptical galaxies show that ellipticals exist up to a redshift of one, but the statistics are too poor to draw firm conclusions concerning the evolution of the population as a whole (see, e.g., Kauffmann et al., 1996; Im et al. 1996; and Im and Casertano 1998). Indirect evidence based on the evolution with redshift of the Fundamental Plane of elliptical galaxies (van Dokkum et al. 1998), on the colors of $z \simeq 0.9$ cluster ellipticals (Stanford et al. 1998), and on the global correlation of metallicity with velocity dispersion (Ziegler & Bender et al. 1997), as well as direct measurement of Balmer line strengths (see, e.g., Bressan et al. 1996), indicate that the stellar populations of ellipticals are old, with ages in excess of 10 Gyrs. Unfortunately, the uncertainties in the basic cosmological parameters do not allow us to firmly convert age estimates into a formation redshift. In particular, if the geometry of our Universe is dominated by a cosmological constant, stars in ellipticals could have formed at a redshift of 1.65 and still be older than 10 Gyrs at the present time (with $\Omega = 0.35$, $\Omega_\Lambda = 0.65$, $H_0 = 65$ km s^{-1} Mpc^{-1}). Stellar-gaseous mergers of disk systems at moderate redshifts appear to reproduce successfully the observed properties of elliptical galaxies (see, e.g., Kauffmann and Charlot 1998 and references therein); in such models, most stars form before the galaxy itself is finally assembled. However, the predictive power of these models is limited by our modest knowledge on star formation processes which are usually treated according to simple empirical relations. On the basis of entirely different theoretical arguments including a detailed description of ISM properties but no cosmology nor dynamical evolution, one could instead argue that spheroidal systems are preferentially formed at high redshift (Spaans & Carollo 1997, Carollo et al. 1997a). Thus, it appears that the present stalemate between different theories and low-to-moderate redshift observations awaits an observational answer.

Important clues may indeed be provided by the discovery of a population of Extremely Red Objects (EROs): relatively bright in the NIR (K$\sim$ 19–20) and very faint in the optical

---

((R−K)> 5 typically [1]). Such a red color can be produced by an "old" stellar population at high redshift (e.g., LBDS 53W091 at z=1.55, Spinrad et al. 1997) or by a younger stellar population enshrouded by dust lanes (e.g., HR10 at z=1.44, Graham & Dey 1996, with one detected emission line). Besides the two prototypical (and particularly bright) cases of LBDS 53W091 and HR10 where it was possible to determine the redshift using the Keck 10-m telescope, the "dust-age" degeneracy in the broad band colors is generally coupled with the redshift and metallicity uncertainties. In other words, the extremely red R-K observed in the EROs can be explained by different combinations of star formation history, redshift, dust content and chemical composition. The only way to photometrically reduce this degeneracy is to obtain multiple broad band colors, over the widest possible spectral range, and to measure morphological properties.

In this Letter we present photometric information of unprecedented completeness about the extremely red $R^{1/4}$ galaxy identified by Treu et al. (1998a) in the Test Image of the Hubble Deep Field South. The new VLT and HDFS data strengthen the early identification as an optimal candidate high redshift elliptical galaxy. If spectroscopically confirmed, this identification would imply that some ellipticals can be in place already at redshift 2 and that their stars have formed at even higher redshifts. In Sect. 2 we describe the observations and the photometric measurements. In Sect. 3 we discuss the identification of the object. In this Letter the Hubble constant is assumed to be 65 km/s/Mpc.

2. Observations

The HDFS NICMOS field was observed with the Test Camera on VLT-UT1 during the VLT Science Verification (Renzini, 1998) and with NICMOS on board the Hubble Space Telescope during the HDFS (Williams et al. 1999) campaign. The field was observed for an additional 9 orbits with the Space Telescope Imaging Spectrograph (STIS) to obtain a broad, high resolution, visible image, and, as one of the flanking fields, with the Wide Field and Planetary Camera 2 (WFPC2). Unfortunately, we were not able to include the WFPC2 images in our analysis as, at the time of this writing, the final reduced frame had not been released. We refer to Fruchter et al. (1999) for the description of the observations and the data reduction.

In the following discussion we shall indicate the Hubble Space Telescope filters in the following way: C = STIS 50CCD (clear); J_{110}= NICMOS F110W; H_{160}= NICMOS F160W; K_{222}= NICMOS F222M.

2.1. Morphology

The galaxy is clearly resolved in the NICMOS and STIS images, as shown in Fig. 1. The light profiles, derived as described by Treu et al. (1998a), are shown in Fig. 2. The shaded areas

---

[1] The definition of EROs is not uniform in the literature. Other values are, for example, (R−K)> 4.5 (Elston et al. 1991) and (R−K)> 6 (Graham & Dey, 1996).
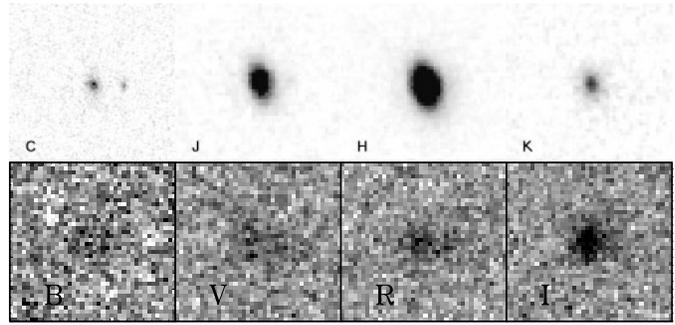
Fig. 1. HST and VLT images of HDFS 223251-603910 **C.** STIS clear. **J.** NICMOS J_{110} **H.** NICMOS H_{160} **K.** NICMOS K_{222}. **B.** VLT B **V.** VLT V **R.** VLT R **I.** VLT I. The images are 3.″75 on a side. A faint blue source very near to the center of the galaxy is visible in the STIS and NICMOS J image.
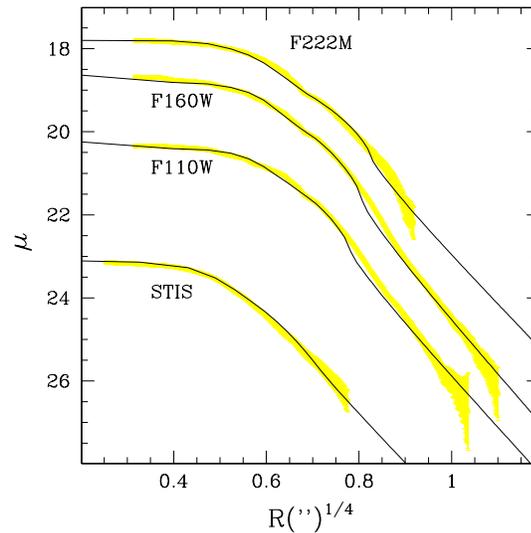
Fig. 2. Luminosity profile of the galaxy (shaded areas) in the STIS and NICMOS passbands. The size of the shaded area is given by the formal error bar. The PSF-convolved best-fit $R^{1/4}$ profile is shown for comparison (solid line).

in the Figure represent the data and the errorbars including the formal error in isophotal fitting and the "sky" subtraction error. The "bumps" present in the observed profiles are mostly due to structures in the PSF (particularly for the NICMOS data). To strenghten the visual classification as an early type galaxy, we fitted the luminosity profile with an $R^{1/4}$ model and an exponential model. We performed the fit independently on each STIS and NICMOS image using two different techniques: the two-dimensional fit code described in Treu et al. (1998b) and the luminosity profile code described in Carollo et al. (1997b). With the latter technique we fitted also a bulge+disk model. We used in each case two different stars as PSFs, in order to check the sensitivity of our results to a particular choice of PSF. We confirm the Treu et al. (1998a) result that only an $R^{1/4}$ profile provides an acceptable fit. The high resolution STIS observations confirm the size we determined from the earlier NICMOS observations; note that the derived half-light radius is larger

Table 1. Photometric properties. For every passband total magnitudes are listed with their errors, except for U and in which case the 95% CL limits is shown. The errors on the magnitudes do not include systematic calibration errors (see Sect. 2.2). The effective radius, as measured by fitting the $R^{1/4}$ profile to the HST images is also listed. The exposure times (texp), the zero points (zp) and colour terms (ct), referred to the ESO and STScI released data, are shown for reference.

Band	$m \pm \delta m$	$r_e \pm \delta r_e$	texp (s)	zp	ct
U	< 26.5	–	17788	31.39	0.239(U-B)
B	29 ± 0.5	–	10200	33.26	0.128(B-V)
V	26.7 ± 0.3	–	14400	33.87	–0.066(B-V)
R	25.81 ± 0.15	–	7200	34.13	–0.061(V-R)
C	25.38 ± 0.15	$0.''26 \pm 0.''06$	25900	26.15	–
I	24.65 ± 0.15	–	10158	33.55	0.023(V-I)
J_{110}	22.01 ± 0.10	$0.''17 \pm 0.''04$	108539	22.16	–
H_{160}	20.47 ± 0.10	$0.''16 \pm 0.''04$	128441	21.52	–
K_{222}	19.33 ± 0.15	$0.''20 \pm 0.''05$	103163	20.00	–

than both the STIS pixel size and PSF FWHM, making our result more robust. The uncertainties listed in Table 1 include the error on the sky subtraction and the error due to PSF estimates. We cannot exclude the presence of a faint, extended disk, but we have verified that our results are not significantly affected by the presence of such disk components by carrying out a variety of bulge+disk fitting experiments (e.g., we find that the "bulge" magnitude does not change by more than ~ 0.1 mag).

2.2. Colors

The multiband colors of HDFS 223251-603910 are summarized in Table 1. The STIS and NICMOS magnitudes are derived by fitting $R^{1/4}$ luminosity profiles as described in the previous Section but were also checked with aperture measurements and found to be consistent to within $\sim$0.1 mags. For the VLT data we give aperture magnitudes corrected for PSF losses. We estimate the systematic error in the correction to be in the range $0.05 - 0.1$ mags. The uncertainties listed (δm) do not include systematic calibration errors, which might be as high as 0.1 mags for the NICMOS magnitudes and as high as 0.05 mags for the VLT magnitudes. We adopt here the NICMOS Pipeline zeropoints. Particularly the H_{160} zeropoint used here is 0.08 mags larger than the one used in Treu et al. (1998a). The VLT zero points in the final coadded images, as released on the WEB site http://www.hq.eso.org/paranal/sv/, were calculated by matching the photometry in the final stacks with that of a single photometric night. The overall consistency of the zeropoints was checked by comparing the VLT data with CTIO data and the main WFPC2 HDFS field. The colors listed in Table 1 are corrected for galactic extinction, using the value E(B-V)=0.026 reported by Schlegel et al. (1998).

3. Discussion of the Spectral Energy Distribution

Before starting the automated best fitting procedure described in the following section we have tried to explore qualitatively

the implications of the observed SED by considering models as young as 1 Myrs and a variety of star formation histories and dust content. Since the SED is relatively flat in both the optical bands (B through I band) and in the near-IR, it is very hard to reproduce it with a combination of a young population and dust obscuration. A combination of an old population with a young population could be tuned to reproduce the observed SED by having the old population providing the near-IR flux and the young population providing the optical flux. This would require the old component to be significantly older than 1 Gyr and thus lead to an even stronger case. Adding dust reddening to such multi-population models would not significantly alter the conclusions on the age of the oldest component. As expected, we find that at fixed redshift, age, metallicity and dust content the reddest models are the single burst ones, which are also the ones better motivated by the observed morphology. As a further check we also compared the colors of HDFS 223251-603910 with the colors of highly reddended starbust galaxies (Calzetti 1998 , and references therein) and we did not find any combination that could reproduce the measured Spectral Energy Distribution.

4. Identification and conclusions

Using nine broad band magnitudes derived from VLT and HST data, we are now able to constrain the SED of ERO HDFS 223251-603910 very well. In order to provide a firm identification, we computed the colors of a large grid of models, with different redshift, age, metallicity and dust content, using the population synthesis code by Bruzual & Charlot (1993, GISSEL96 version). On the basis of the qualitative investigation described in the previous section we have focussed most of our efforts on single burst stellar populations. Specifically we considered models with metallicity $Z/Z_{\odot}$=1,0.4,0.2 and dust reddening A_V=0,0.5,1 (using the extinction law from Cardelli et al. 1989). The IMF is a Salpeter IMF between 0.1 and 125 $M_{\odot}$. Here, we considered stellar population ages down to 250 Myrs, with a roughly uniform spacing in age. We computed the χ^2 of each model fitted to the observed SED. In Fig. 3 the contour levels of probability 68, 80 and 95% are shown. In the nine panel the metallicity decreases from left to right, while the dust reddening increases from top to bottom. As can be seen, the redshift is relatively well constrained, but the age of the object is much more uncertain. This is a consequence of the so-called age-metallicity degeneracy (e.g., Worthey, 1994), i.e., that broad band colors cannot distinguish the effects of age and metallicity. Only spectroscopy could constrain both the metal content and the age of the object. The dotted and dashed lines on the upper left corner of the plots are the age of Universe as a function of redshift (h=0.65; dotted: $\Omega = 1, \Omega_{\Lambda} = 0$, dashed: $\Omega = 0.3, \Omega_{\Lambda} = 0.7$). As the galaxy cannot be older than the Universe, only the region below the curves is allowed. The best fitting models of our grid in the cases $A_v = 0, 0.5$ and $Z/Z_{\odot}$=1,0.4 are shown in Fig. 4, together with the photometric points. The χ^2 and the model characteristics are also shown in the figure.
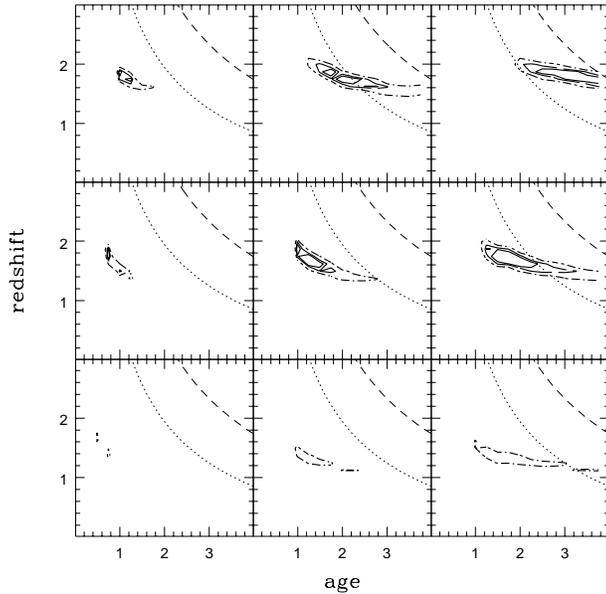
Fig. 3. Contour plots of the χ^2. The colors of a grid of models (see text for details) have been computed and compared with the observed ones. The age is given in Gyrs. The metallicity of the stellar populations is $Z/Z_\odot$=1,0.4,0.2 from left to right, the dust reddening is A_V=0,0.5,1 from top to bottom. The contours correspond to a probability of 68, 80 and 95% from the inside to the outside. The two curves in the upper left corner represent the age of the Universe as a function of redshift for two different cosmologies (see text). The object must be younger than the Universe and therefore only the region below the curves is allowed. Its redshift is better constrained than its age.
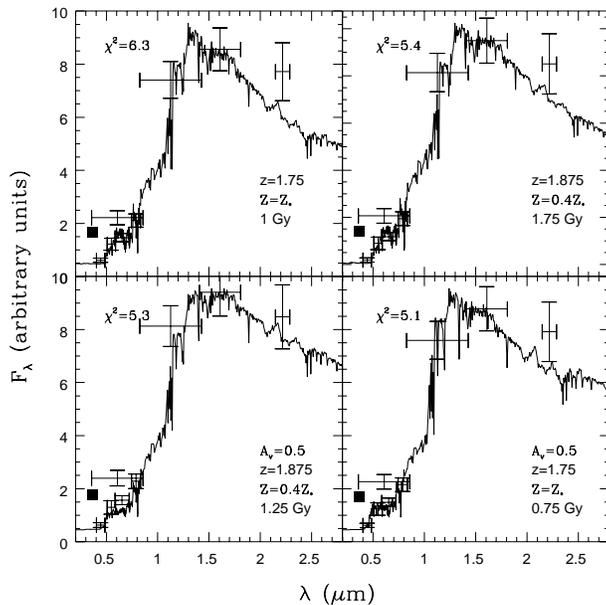
Fig. 4. The best fitting spectra for the cases with Z=1,0.4$Z_\odot$ and $A_V = 0, 0.5$ are shown, together with the observed photometric measurements and the values of the χ^2. The filled square is the U band VLT upper limit. The error bars on the wavelength axis represent the filter bandwidths. The main contribution to STIS CCD clear filter comes from the reddest part of the spectrum. The χ^2 with seven degrees of freedom is shown in the upper left corner.

As already noticed in Treu et al. (1998a), the luminosity of this galaxy is consistent with its identification as an elliptical galaxy at $z \simeq 1.8$, e.g., for $\Omega = 0.35$ and $\Omega_\Lambda = 0.65$, the galaxy would have, after passive dimming down to z=0, $M_V \simeq -21.4$ ($M_V \simeq -24$ without passive dimming) and an effective radius of about 4 kpc.

Thus, all the photometric data collected so far are consistent with the identification of this object as a high redshift elliptical. This renders HDFS 223251-603910 a prime target for spectroscopic followup (see Benitez et al. 1998, Fontana et al. 1999 for additional candidates in the same field). This is within reach with IR spectrograph on 8m class telescopes, such as ISAAC on the VLT. If confirmed, its identification will demonstrate that ellipticals can already be assembled at redshift almost 2. Furthermore, by measuring its absorption line strengths we will determine in great detail its physical properties, such as age, metal content and star formation history, thus improving our knowledge of the early stages of galaxy formation.

References

Benitez N., Broadhurst T., Bouwens R., Silk J., Rosati P., 1998, astro-ph/9812205
Bressan A., Chiosi C., Tantalo R., 1996, A&A, 311, 425
Bruzual A. G., Charlot S. 1993, ApJ, 405, 538
Calzetti D., 1998, astro-ph/9806083
Cardelli J., Clayton G., Mathis J. 1989, ApJ, 345, 245
Carollo C. M., Spaans M., Stiavelli M., Mihos J. C., 1997, in "Science with the NGST", E.P. Smith and A. Koratkar eds, p. 237.
Carollo C. M., Franx M., Illingworth G. D., Forbes D. A. 1997b, ApJ, 481, 710
Elston R., Rieke G. H., Rieke M. J. 1991, in Elston (ed.):"Astrophysics with Infrared Arrays", ASP, San Francisco.
Fontana A., et al., 1999, submitted to AAL
Fruchter A. S., et al., 1999, in preparation
Graham J. R., Dey A. 1996, ApJ, 471, 720
Im M., Griffiths R., Ratnatunga K.U., Sarajedini V.L., 1996, ApJ, 461, L79
Im M., Casertano S., 1998, preprint.
Kauffmann G., Charlot S., 1998, MNRAS, 294, 705
Kauffmann G., Charlot S., White S.D.M., 1996, MNRAS, 283, L117
Renzini, 1998, ESO Messenger, 93, 1
Schlegel D.J. et al. 1998, ApJ, 500, 525
Spaans M., Carollo C.M., 1997, ApJ, 482, 93
Spinrad H., Dey A., Stern D., et al. 1997, ApJ, 484, 581
Stanford S. A., Eisenhardt P. R., Dickinson M., 1998, ApJ, 492, 462
Treu T., Stiavelli M., Walker A. R., et al. 1998a, AA, 340, L10.
Treu T., Stiavelli M., Casertano S., et al. 1998b, submitted to MNRAS
van Dokkum P., Franx M., Kelson D., Illingworth, G. D. 1998, ApJL, 504, 17
Williams R. E. et al. 1999, in preparation
Worthey G., 1994, ApJS, 95, 107
Ziegler B.L., Bender R., 1997, MNRAS, 291, 527